ACCOUNTS of chemical research

Article

Cite This: Acc. Chem. Res. 2019, 52, 1979−1989

pubs.acs.org/accounts

Magnesium for Dynamic Nanoplasmonics

Xiaoyang Duan[†,‡] and Na Liu*[,†,‡]

[†]Max Planck Institute for Intelligent Systems, Heisenbergstrasse 3, D-70569 Stuttgart, Germany

[‡]Kirchhoff Institute for Physics, University of Heidelberg, Im Neuenheimer Feld 227, D-69120, Heidelberg, Germany

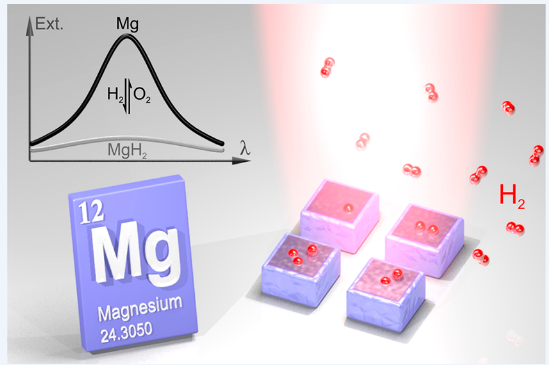

CONSPECTUS: The key component of nanoplasmonics is metals. For a long time, gold and silver have been the metals of choice for constructing plasmonic nanodevices because of their excellent optical properties. However, these metals possess a common characteristic, i.e., their optical responses are static. The past decade has been witnessed tremendous interest in dynamic control of the optical properties of plasmonic nanostructures. To enable dynamic functionality, several approaches have been proposed and implemented. For instance, plasmonic nanostructures can be fabricated on stretchable substrates or on programmable templates so that the interactions between the constituent metal nanoparticles and therefore the optical responses of the plasmonic systems can be dynamically changed. Also, plasmonic nanostructures can be embedded in tunable dielectric materials, taking advantage of the sensitive dependence of the localized surface plasmon resonances on the neighboring environment. Another approach, which is probably the most intriguing one, is to directly regulate the carrier densities and dielectric functions of the metals themselves.

In this Account, we discuss a relatively new metal in nanoplasmonics, magnesium, and its important role in the development of dynamic plasmonic nanodevices at visible frequencies. We first elucidate the basic optical properties of Mg and compare it with conventional plasmonic materials such as Au, Ag, and others. Then we describe a unique characteristic of Mg, i.e., its reversible phase transitions between the metallic state and a dielectric state, magnesium hydride, through hydrogenation and dehydrogenation. This sets the basis for Mg in dynamic nanoplasmonics. In particular, the structural properties and dielectric functions of the two distinct states are discussed in detail. Subsequently, we highlight the experimental investigations of the physical mechanisms and nanoscale understanding of Mg nanoparticles during hydrogenation and dehydrogenation. We then introduce a plethora of newly developed Mg-based dynamic optical nanodevices for applications in plasmonic chirality switching, dynamic color displays with Mg nanoparticles and films, and dynamic metasurfaces for ultrathin and flat optical elements. We also outline strategies to enhance the stability, reversibility, and durability of Mg-based nanodevices. Finally, we end this Account by outlining the remaining challenges, possible solutions, and promising applications in the field of Mg-based dynamic nanoplasmonics. We envision that Mg-based dynamic nanoplasmonics will not only provide insights into understanding the catalytic processes of hydrogen diffusion in metals by optical means but also will open an avenue toward functional plasmonic nanodevices with tailored optical properties for real-world applications.

■ INTRODUCTION

The beautiful colors exhibited by metal nanoparticles have been known since medieval times. Artisans exploited the effect to create colorful glass long before the underlying mechanisms were understood. This phenomenon results from the absorption of sunlight by the metal particles embedded in glass. At a specific wavelength that depends on the size, shape, and environment of the nanoparticle collective oscillations of the conduction electrons, so-called localized surface plasmon resonances (LSPRs), takes place.[1,2] LSPRs confine the incident field near the nanoparticle at dimensions much smaller than the operating wavelength. This leads to a strong enhancement of the local fields and allows for manipulation of light below the optical diffraction limit. Such characteristics enable a variety of applications in different disciplines, including physics, chemistry, biology, materials science, and others.[2−9]

For a long time, the development of plasmonics has been focused on static systems, whose optical properties are fixed once the structures are fabricated. The concept of active plasmonics or dynamic plasmonics was first proposed in 2004 for controlling signals in a waveguide using nanoscale structural transformations.[10] Since then, the research interest along this direction has flourished. Dynamic plasmonics has taken off as a burgeoning subfield of plasmonics, identifying an inevitable transition of plasmonics from static to dynamic.[11,12] In general, there are two distinct routes to dynamic modulation of the optical properties of plasmonic systems. The first is tuning of the conformations of the plasmonic structures so that the interactions between the constituent metal nanoparticles can be dynamically changed. This is not straightforward for

Received: March 28, 2019
Published: June 27, 2019

DOI: 10.1021/acs.accounts.9b00157
Acc. Chem. Res. 2019, 52, 1979−1989

lithographically fabricated samples, as the structures are generally restricted on substrates. However, bottom-up approaches such as dynamic DNA nanotechnology provide elegant solutions.[6,13−15] The second is tuning of the LSPRs of the individual metal nanoparticles by varying their dielectric surroundings or directly regulating the carrier densities and dielectric functions of the metal particles themselves. For the former, materials that can serve as tunable dielectric surroundings are quite versatile. This includes optically active materials such as photochromic molecules,[16] J-aggregates,[17] quantum dots,[5] and perovskites,[18] thermoresponsive materials such as gallium,[10] vanadium oxide,[19] and germanium antimony telluride,[20] and electrically driven materials such as liquid crystals[21] and graphene,[22] among others. For the latter, metals that can be regulated directly and meanwhile exhibit excellent plasmonic properties are not very numerous, especially in the visible spectral range.[23−25]

Magnesium is one of the promising candidates, as it exhibits excellent optical properties at high frequencies and can absorb/desorb hydrogen, undergoing reversible transitions between metal and dielectric hydride (MgH_2) states.[23,26] This offers great opportunities to design and construct dynamic optical nanodevices at visible frequencies. In this Account, we elucidate the power of Mg for dynamic nanoplasmonics. More specifically, we first evaluate the plasmonic and dynamic properties of Mg. We then discuss the physical mechanisms and nanoscale understanding of Mg nanoparticles during hydrogenation and dehydrogenation. Subsequently, a plethora of newly developed Mg-based dynamic optical nanodevices are introduced and reviewed. This includes applications in plasmonic chirality switching, dynamic color displays with Mg nanoparticles and films as well as dynamic metasurfaces for ultrathin and flat optical elements. We also discuss strategies to enhance the stability, reversibility, and durability of Mg-based nanodevices. Finally, we end this Account with a conclusion and outlook.

PLASMONIC PROPERTIES OF MG

The dielectric function of bulk metals can be described by the Drude model:[27]

$$\varepsilon(\nu) = \varepsilon_r(\nu) + i\varepsilon_i(\nu) = \varepsilon_\infty - \frac{{\nu_p}^2}{\nu(\nu + i\gamma)} + \varepsilon_{inter}(\nu) \tag{1}$$

where $\varepsilon_r(\nu)$ and $\varepsilon_i(\nu)$ are the real and imaginary parts of the dielectric function, ε_∞ is the high-frequency-limit dielectric constant, ε_{inter} represents the contribution from interband transitions, γ is the damping constant, and ν_p is the plasma frequency. In the quasistatic regime, where the particle size is much smaller than the wavelength of light in the surrounding medium (i.e., $d \ll \lambda$), the condition for resonance, known as the Fröhlich condition,[27] is fulfilled at $\varepsilon_r = -2$ for a Drude metal sphere located in air. The Fröhlich frequency, $\nu_f \approx \nu_p/\sqrt{3}$, is the frequency at which the LSPR can be excited in the metal sphere. The figure of merit, which characterizes the quality of the excited LSPR, can be written as[24]

$$Q_{LSP} = \frac{\nu}{\Delta\nu} \approx -\frac{\varepsilon_r(\nu)}{\varepsilon_i(\nu)} \tag{2}$$

Sanz et al. systemically compared the LSPR positions (Fröhlich energies $E_f = h\nu_f$) and values of Q_{LSP}^{max} for different metals, including Mg, Au, Al, Ag, and others, as shown in Figure 1.[23]

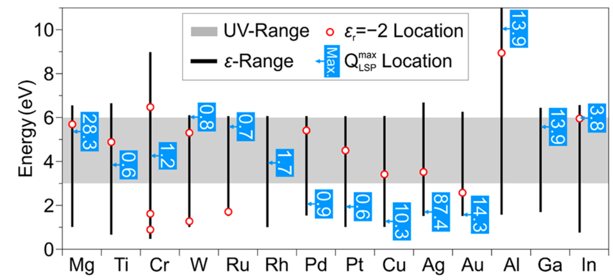

Figure 1. Evaluation of the plasmonic properties of different metals. The Fröhlich energy and the maximum plasmonic performance value, Q_{LSP}^{max}, are plotted at the spectral position where they are achieved. Reproduced from ref 23. Copyright 2013 American Chemical Society.

In general, metals with small $\varepsilon_i(\nu)$ present strong and narrow resonances. It is apparent that Mg has excellent plasmonic properties, superior to those of most of the metals (see Figure 1). More specifically, compared with conventional plasmonic materials such as Au, Ag, and Al, Mg can produce sharper resonances than Au and Al but is not as good as Ag. Nevertheless, Mg is a more promising material for UV plasmonics than Ag, as interband transitions for Ag already start near 4 eV. On the contrary, Mg has no d-shell electrons, and thus, no interband transitions involving d-shell electrons occur.[28]

DYNAMIC PROPERTIES OF MG

Mg reacts reversibly with hydrogen to form magnesium hydride[26,29] according to the reaction: $Mg + H_2 \rightleftarrows MgH_2 + 75.2\ kJ\ mol^{-1}$. MgH_2 is an ionic compound with an appreciable covalent contribution. It exhibits a charge density distribution of $Mg^{+1.91}\ H^{-0.26}$, in which Mg is almost fully ionized but H is very weakly ionized.[30] The diffusing species in Mg is the H^- anion, whose diffusion rate is much lower than that of H^+ in vanadium, niobium, and palladium.[31]

Mg has a hexagonal close-packed (hcp) structure with lattice parameters $a_1 = a_2 = a_3 = 3.21$ Å and $c = 5.21$ Å (see Figure 2A).[32,33] Previous studies showed that for Mg films and particles deposited on substrates without lattice matching, for instance, on glass, silicon, aluminum oxide, and titanium, they attained energetically favorable orientations determined by the interface energies, where the facets corresponded to the closest-packed planes.[34−36] In other words, the hexagonal prism is the most preferable shape with the Mg [0001] direction perpendicular to the substrate plane.[34] When a small quantity of hydrogen dissolves into the Mg crystal lattice, the α-MgH_x phase (interstitial solid solution of H in Mg) is formed, and it has a hexagonal crystal structure.[29,37] Upon further hydrogenation, β-MgH_2 with a tetragonal rutile crystal structure forms, with lattice parameters $a = b = 4.52$ Å and $c = 3.02$ Å (see Figure 2A).[32,33] In between these two phases there exists a mixed region, the $\alpha+\beta$ phase, in which hydrogen dissolved in Mg is in equilibrium with MgH_2. The plateau pressure for the transition from the α phase to the $\alpha+\beta$ phase is 0.41 Torr at 353 K.[29] Electron diffraction studies revealed that the most intrinsic orientation relationship between the Mg and MgH_2 lattices during the phase transition was $Mg(0001)[2\bar{1}\bar{1}0] \parallel MgH_2(110)[001]$ (see the insets in Figure 2A).[32,33] Because

DOI: 10.1021/acs.accounts.9b00157
Acc. Chem. Res. 2019, 52, 1979−1989

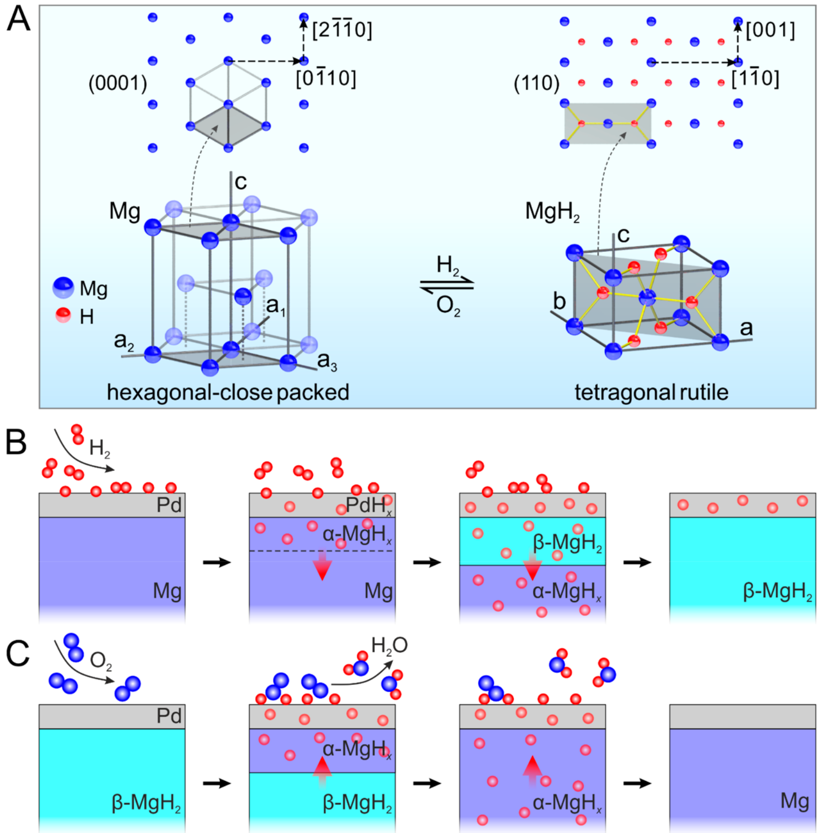

Figure 2. (A) Crystallographic phase transformations between Mg and MgH_2. The insets show the atomic arrangements in the Mg(0001) and MgH_2(110) planes, respectively, which are parallel to the substrate. (B, C) Schematic models of the (B) hydrogenation and (C) dehydrogenation processes for Pd-capped Mg upon hydrogen and oxygen exposure, respectively.

of the atomic movements resulting from the phase transition, the distance between the Mg atoms is expanded by 23% (from c_{Mg} to $\sqrt{2}\,a_{MgH_2}$) along the direction perpendicular to the substrate plane. The distance between the Mg atoms in the substrate plane is expanded by only 6%. Hence, major lattice distortions occur along the out-of-plane direction.[38]

Mg is a potential material for solid-state hydrogen storage because of its abundance, low cost, reversibility, and large gravimetric (7.6 wt %) and volumetric (110 g L^{-1}) hydrogen capacities.[26] However, there are two major obstacles for practical applications: high hydrogenation/dehydrogenation temperatures and sluggish hydrogen absorption/desorption kinetics. The surface of pure Mg has a large activation energy for hydrogen dissociation and hydride formation. Hydrogenation of Mg requires high operating temperatures (up to ~300 °C at 1 atm pressure), and dehydrogenation needs even higher temperatures (~400 °C).[39,40] It was discovered that capping of Mg with Pd can reduce the high operating temperatures to ambient conditions by catalyzing the dissociation of H_2 molecules.[40] In this case (see Figure 2B), as the reaction progresses MgH_2 grows at the Mg–Pd interface. The kinetic limiting step is hydrogen diffusion through the growing MgH_2 layer, which acts as a barrier for further hydrogenation of Mg. This is the so-called blocking effect.[41] During dehydrogenation, the growing metallic Mg near the Mg–Pd interface then limits the desorption kinetics (see Figure 2C).

MgH_2 is a transparent and color-neutral insulator with a band gap of 5.6 ± 0.1 eV.[42] MgH_2 can be regarded as a nearly nondispersive and low-loss dielectric material with refractive index $n + ik = 1.95 + i0.01$ in the visible and near-infrared regimes.[42] As a result of the large contrast between Mg and MgH_2 in both optical and electrical properties, the transition processes can be conveniently investigated by joint optical and electrical measurements in real time.[43]

■ DYNAMIC PLASMONIC NANOPARTICLES

In 1997, van der Sluis et al. demonstrated optical switching of Mg-based films between mirror and transparent states through hydrogenation and dehydrogenation.[44] Since then, "switchable mirrors" have been widely investigated. This has led to a variety of applications, including optical hydrogen sensors,[45] switchable solar absorbers,[46] and smart windows.[47] However, the blocking effects as a bottleneck problem remained, hampering further development for practical applications. Later, Uchida et al. showed that Mg films exhibited favorable absorption kinetics only for film thicknesses below ~100 nm, with a diffusion coefficient of $\sim 10^{-16}$ m^2 s^{-1}.[37] Subsequently, a MgH_2 layer was formed at the Mg–Pd interface, and the diffusion coefficient decreased to $\sim 10^{-18}$ m^2 s^{-1}, preventing hydrogen from effective diffusion. Although the kinetics could be improved by increasing the temperature and/or decreasing the hydrogen concentration,[41] the formation of MgH_2 as a diffusion barrier dramatically slowed down the diffusion process, especially when the diffusion length was longer than ~100 nm.

To enhance the diffusion kinetics, Mg and MgH_2 particles have been utilized.[48] Small particles possess higher surface-to-volume ratios than large particles, giving rise to higher reaction

DOI: 10.1021/acs.accounts.9b00157
Acc. Chem. Res. 2019, 52, 1979–1989

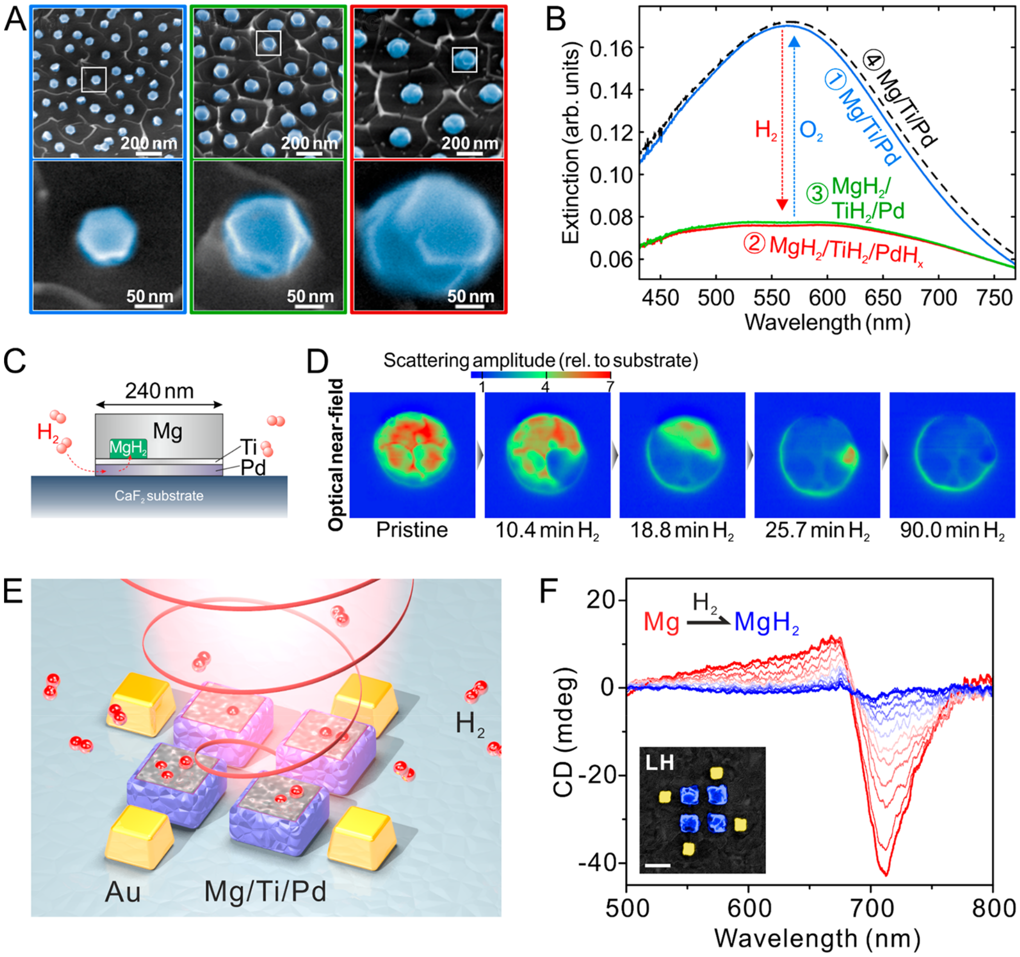

Figure 3. (A) Colorized SEM images of Mg nanodisks with different diameters. (B) Extinction spectra of the 80 nm Mg/5 nm Ti/10 nm Pd particles with a diameter of 160 nm in the different stages of a typical hydrogenation/dehydrogenation cycle. (C) Schematic of the Mg nanostructure, consisting of 40 nm Mg/5 nm Ti/10 nm Pd. (D) Near-field scattering maps of the Mg particle recorded between hydrogen exposures, covering an area of 600 nm × 600 nm. (E) Schematic of a hybrid chiral plasmonic system consisting of four Mg/Ti/Pd particles and four Au particles in a gammadion-like arrangement. (F) Evolution of the measured CD spectra upon hydrogen loading as a function of time. Scale bar: 200 nm. Reproduced from (A, B) ref 50, (C, D) ref 51, and (E, F) ref 61. Copyright 2015, 2018, and 2016, respectively, American Chemical Society.

rates. Decreasing the crystal grain size can also reduce the thermodynamic stabilities of Mg and MgH_2, resulting in lower hydrogen absorption and desorption temperatures.[49] The most common method for producing Mg particles is mechanical milling. However, the lack of quantitative control over the size, morphology, and composition has encumbered the understanding of hydrogenation/dehydrogenation mechanisms on the nanoscale.

In recent years, advances in nanofabrication techniques have offered great opportunities to pattern Mg nanoparticles with controlled sizes, shapes, compositions, and surface morphologies. This has also enabled a wealth of Mg-based plasmonic nanostructures. For instance, Sterl et al. fabricated Mg nanoparticles of various sizes by colloidal hole−mask lithography and subsequent electron-beam evaporation (see Figure 3A).[50] These Mg particles possessed a hexagonal monocrystalline shape when their size was relatively small (~100 nm) but tended to be polycrystalline with increasing size. These Mg nanoparticles also exhibited pronounced LSPRs, which could be tuned throughout the visible wavelength range by varying the particle size. With the help of Pd as a catalytic layer, the resonances could be turned off/on upon hydrogen/oxygen exposure at room temperature, when the particles were transformed between the metallic Mg state and the dielectric MgH_2 state (see Figure 3B). The weak resonances still observable in the MgH_2 state mainly resulted from incomplete hydrogenation of the Mg particles. To avoid Mg−Pd alloy formation,[39] 5 nm Ti was used to separate Mg and Pd. This buffer layer also helped to release the mechanical stress resulting from the different expansion rates of Mg and Pd upon hydrogen absorption.

NANOSCALE HYDROGENOGRAPHY ON SINGLE MG NANOPARTICLES

The spatial resolution of conventional hydrogenography in the horizontal plane is optical-diffraction-limited. This prevents direct optical investigations of hydrogen diffusion in individual Mg crystallites, which are typically on the size scale of 100 nm. To understand hydrogenation of Mg particles on the nanoscale, Sterl et al. utilized scattering-type scanning near-field optical microscopy (s-SNOM), which can locally probe the dielectric properties of matter with a spatial resolution on the order of tens of nanometers.[51] Dark-field spectroscopy was employed to measure the scattering spectra of single Mg

DOI: 10.1021/acs.accounts.9b00157
Acc. Chem. Res. 2019, 52, 1979−1989

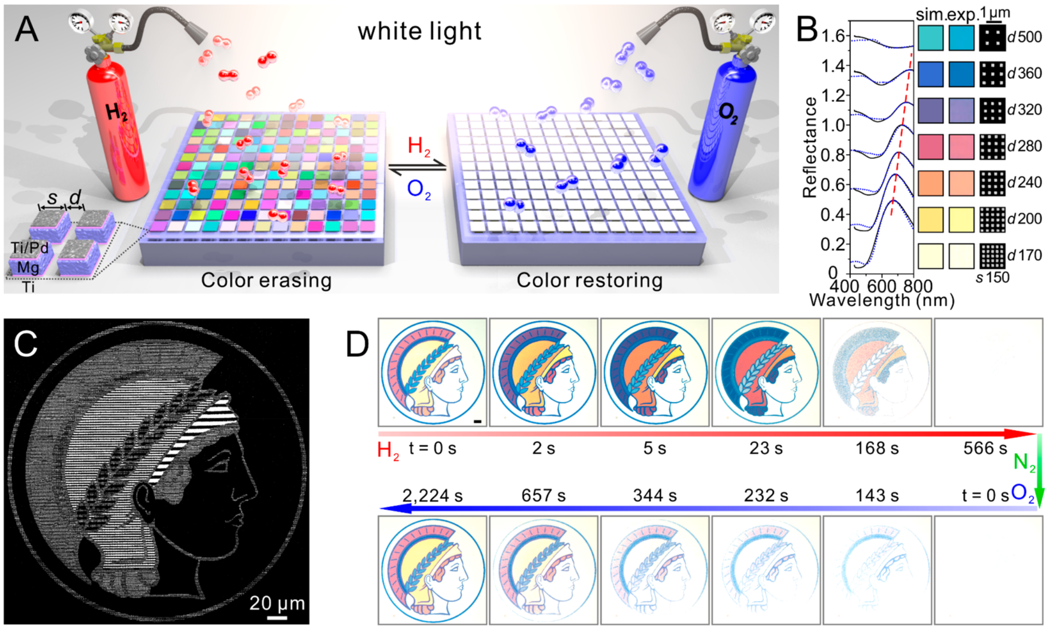

Figure 4. (A) Schematic of the plasmonic metasurface composed of Mg nanoparticles. (B) Experimental (black) and simulated (blue dotted) reflectance spectra and colors as well as the corresponding SEM images of the structures. (C) Overview SEM image of the Minerva logo sample. (D) Optical micrographs of the Minerva logo during hydrogenation and dehydrogenation for color tuning, erasing, and restoring. Scale bar: 20 μm. Reproduced with permission from ref 64. Copyright 2017 Nature Publishing Group.

particles, which were used to evaluate the amount of metallic Mg within each particle.

The s-SNOM images recorded after different H_2 exposure durations (see Figure 3D) revealed that the hydrogenation process was inhomogeneous both temporally and spatially in the Mg nanoparticles. The phase transition from Mg to MgH_2 was rapid within a single crystallite before progressing toward adjacent ones. Each particle exhibited an individual hold-back time in the beginning. This could be attributed to the grain boundaries of the individual crystallites, which acted as barriers for hydrogen diffusion in a single nanostructure.[52] This work proved that the crystalline structure of Mg nanoparticles is crucial for the hydrogen absorption and desorption kinetics, providing insights into the design and fabrication of Mg-based dynamic optical nanodevices.

PLASMONIC CHIRALITY TUNING

Chirality is a geometrical property of an object. A chiral object and its mirror image are called enantiomers, and they cannot be superimposed on one another. Apart from geometrical properties, chirality can also manifest itself optically via a different response to left- and right-handed circularly polarized (LCP and RCP) light. The resulting absorption difference is called circular dichroism (CD).[53] In general, the CD of natural chiral molecules such as amino acids, proteins, carbohydrates, etc. is very weak and located only in the UV spectral region.[53] In contrast, chiral plasmonic structures can exhibit spectrally tunable and pronounced CD that is several orders of magnitude larger than that of natural chiral molecules.[54−60]

We demonstrated a hydrogen-regulated chiral plasmonic system as shown in Figure 3E.[61] Each chiral structure consisted of four Au and four Mg particles that were arranged in a gammadion-like geometry. The Mg particles were capped with 5 nm Ti and 10 nm Pd to facilitate hydrogen loading/unloading at room temperature. The samples were fabricated using a double electron-beam lithography (EBL) process. Its scanning electron microscopy (SEM) image is shown in Figure 3F.

Before hydrogen loading, the left-handed sample exhibited a bisignate spectral profile, as characterized by the red line in Figure 3F. This resulted from the resonant coupling between the collective plasmons excited in the eight plasmonic particles.[62] Upon hydrogen loading, Pd catalyzed the dissociation of hydrogen molecules into atoms, which could diffuse through the Ti spacer into the Mg particles. As a result, the four Mg particles were gradually hydrogenated to form MgH_2 particles. This was reflected by the successively decreasing CD strength. In the end, the entire structure became achiral, giving rise to a featureless CD spectrum. The chiral spectra could be recovered through dehydrogenation by exposing the sample to ambient air or oxygen. Hence, the chiroptical responses of the plasmonic structures could be dynamically switched off/on simply by hydrogenation/dehydrogenation. Such a dynamic control concept may lead to plasmonic chiral platforms for a variety of gas detection schemes by exploiting the high sensitivity of CD spectroscopy. It is noteworthy that in ambient air Mg can form MgO with oxygen and magnesium hydroxycarbonate with carbon dioxide and possibly become hydroxylated to form $Mg(OH)_2$. This results in low system reversibility for only several cycles. The reversibility can be improved by carrying out the experiment in a dry environment and/or covering the Mg surface with a thin poly(tetrafluoroethylene) protection layer.

DYNAMIC PLASMONIC COLOR DISPLAYS BASED ON MG NANOPARTICLES

Plasmonic color generation based on engineered metasurfaces has stimulated a variety of fascinating applications in color display science for high-density optical data storage, information anticounterfeiting, and data encryption.[7,63] Using catalytic Mg metasurfaces as shown in Figure 4A, we demonstrated a dynamic plasmonic display technique that

DOI: 10.1021/acs.accounts.9b00157
Acc. Chem. Res. 2019, 52, 1979−1989

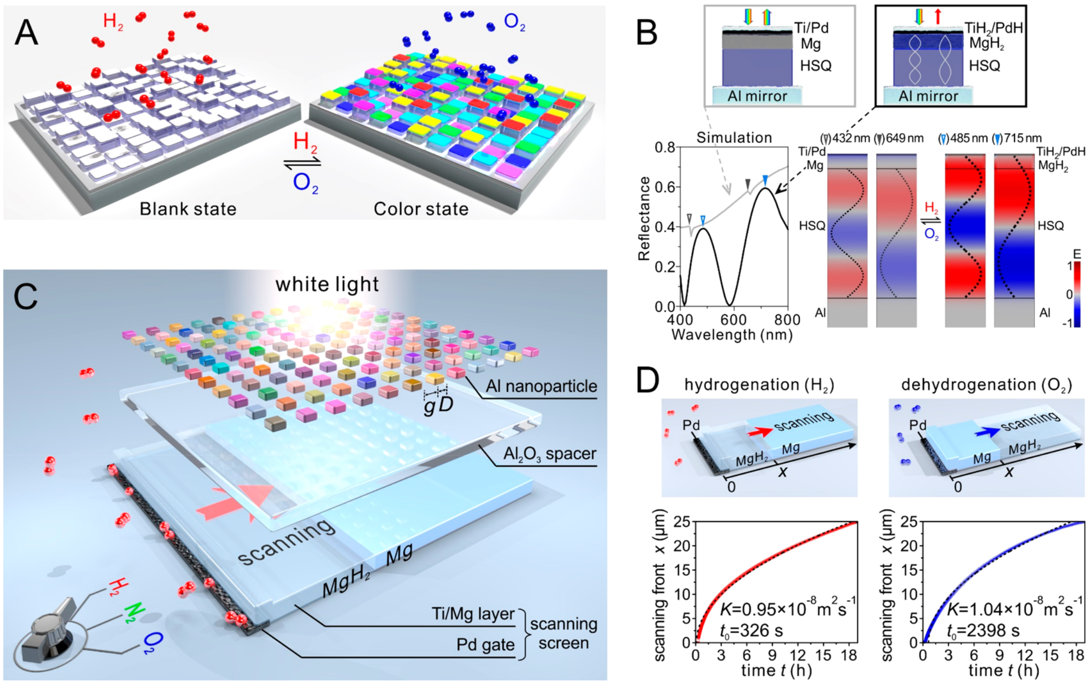

Figure 5. (A) Schematic of the dynamic color display using stepwise FP resonators. Pixelated HSQ pillars of different heights generated by grayscale nanolithography are sandwiched between a Mg/Ti/Pd (50 nm/2 nm/3 nm) capping layer and an Al mirror. (B) Simulated reflectance spectra of a representative FP resonator in the blank (gray line) and color (black line) states, respectively. The electric field distributions of the different FP resonances (highlighted using arrows) before and after hydrogenation are also shown. (C) Schematic of the scanning plasmonic color display, consisting of Al nanoparticles as plasmonic pixels, a 20 nm dielectric Al_2O_3 spacer, and a scanning Mg screen (15 μm × 15 μm × 30 nm) with a 3 nm Ti buffer layer. (D) Scanning front x of the Mg screen during hydrogenation (red) and dehydrogenation (blue) at different times as tracked by in situ optical hydrogenography. Reproduced from (A, B) ref 65 and (C, D) ref 66. Copyright 2017 and 2018, respectively, American Chemical Society.

enabled the fabrication of plasmonic microprint displays with good reversibility.[64]

The plasmonic pixels comprising Mg nanoparticles were sandwiched between Ti/Pd capping layers and a Ti buffer layer. On the metasurface, these Mg particles were arranged in a lattice with various particle sizes and interparticle distances to achieve brilliant colors in a broad range (see Figure 4B). Through hydrogenation, different-colored squares underwent a series of vivid color changes until all of the colors vanished. The hydrogenation process was essentially associated with a gradual decrease of the metallic fraction of the particles, forming MgH_2 as a dielectric surrounding. Such a catalytic process rendered dynamic alterations to the reflectance spectra and therefore the exhibited colors possible.

A plasmonic microprint based on the Max Planck Society's Minerva logo was fabricated, as shown in Figure 4C. Upon hydrogen loading, the Minerva logo experienced dynamic color changes. Abrupt color alterations took place within 23 s. Subsequently, the logo started to fade and completely vanished after 566 s. Upon oxygen exposure, the logo could be restored to its starting state. We further showed that through smart material processing, information encoded on selected pixels, which were indiscernible to both optical and scanning electron microscopies, could be read out using hydrogen as a decoding key, suggesting a new generation of information encryption and anticounterfeiting applications.

DYNAMIC COLOR DISPLAYS BASED ON MG CAVITY RESONANCES

To simplify the fabrication procedures and enhance the durability of Mg-based dynamic displays, we reported a dynamic color display scheme using pixelated Fabry−Pérot (FP) cavities (see Figure 5A).[65] Each pixel (500 nm × 500 nm) consisted of a dielectric hydrogen silsesquioxane (HSQ) pillar sandwiched between an Al mirror and a metallic capping layer composed of Mg/Ti/Pd (50 nm/2 nm/3 nm). By tuning of the pillar heights using grayscale lithography, a series of FP cavities were formed.

Before hydrogenation, the Mg/Ti/Pd capping layer efficiently reflected the visible light, resulting in no color generation. This defined a blank state (see Figure 5B). Upon hydrogen exposure, as Mg was gradually transformed into MgH_2, the effective thickness of the metallic capping layer decreased, and light started to be transmitted through it. When Mg was fully hydrogenated into MgH_2, colors were selectively reflected from these FP resonators of different heights. In this case, each FP resonator consisted of a TiH_2/PdH capping layer, a double dielectric spacer (MgH_2 + HSQ), and an Al back mirror. Such asymmetrical FP resonators with ultrathin lossy capping generated vivid and high-contrast colors with a wide gamut, representing a color state. The resonance properties, such as the reflectance peak positions and the number of allowed modes in the FP resonators, were largely governed by the individual cavity heights, as shown in Figure 5B. This scheme utilized a Mg layer directly from thin-film deposition to achieve dynamic color changes without any post-nanofabrication steps.

DOI: 10.1021/acs.accounts.9b00157
Acc. Chem. Res. 2019, 52, 1979−1989

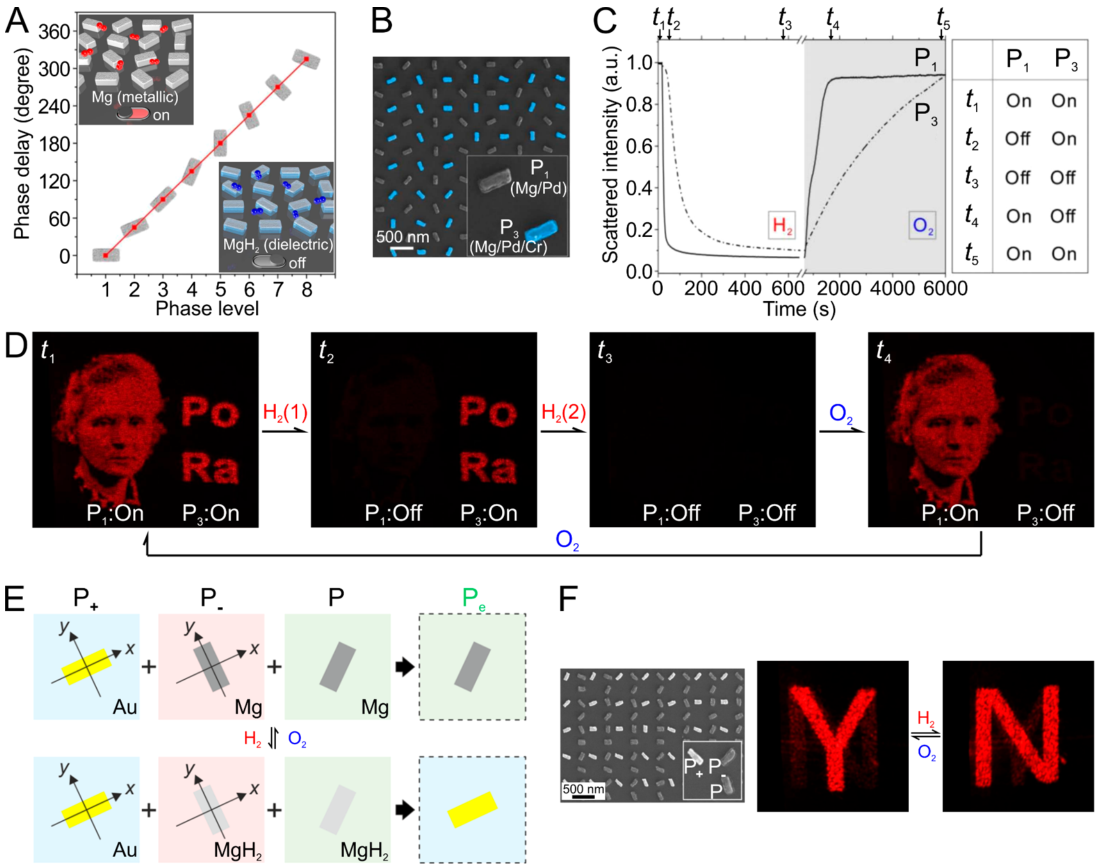

Figure 6. (A) Schematic of the metasurface hologram consisting of Mg nanorods with different orientations and the simulated phase delay with respect to the orientation. (B) Overview SEM image of the hybrid metasurface. (C) Evolution of the scattered intensities of P_1 (solid line) and P_3 (dash-dotted line) during hydrogenation and dehydrogenation. (D) Representative snapshots of the holographic images during hydrogenation and dehydrogenation. (E) Working principle of the dynamic Janus metasurface. (F) Snapshots of the holographic images before and after hydrogenation. (A−D) Reproduced with permission from ref 70. Copyright 2018 AAAS. (E, F) Reproduced from ref 71. Copyright 2018 American Chemical Society.

■ SCANNING PLASMONIC COLOR DISPLAYS

Very recently, we demonstrated a novel scanning plasmonic color display, taking inspiration from macroscopic scanning devices.[66] As shown in Figure 5C, the microscopic scanning screen was a Ti/Mg (5 nm/30 nm) layer with dimensions of 15 μm × 15 μm on a SiO_2 substrate. To enable the scanning characteristics, the left side of the screen was in contact with a Pd strip, which worked as a gate for hydrogen loading or unloading. Al nanoparticles, i.e., the plasmonic pixels, were arranged on top of the scanning screen, spaced by a 20 nm Al_2O_3 layer. Upon hydrogen loading, hydrogenation of Mg started from the Pd gate, such that the plasmonic pixels were laterally scanned following the hydrogen diffusion direction. During the process, the scanning screen transited from a mirror (Mg) to a transparent spacer (MgH_2). This process was reversible through dehydrogenation using oxygen.

In particular, we carefully investigated lateral hydrogen diffusion in Mg,[67] which had rarely been studied before. In contrast to the vertical diffusion scheme (i.e., out-of-plane diffusion),[26,29,37] we discovered that the blocking effects were absent in long-range lateral diffusion over tens of micrometers. In addition, the lateral diffusion was fast at all times and not hampered by the MgH_2 barrier layer. In order to characterize the mobility of the diffusion front, optical hydrogenography was utilized to record optical reflection images of the diffusion process in situ. As shown in Figure 5D, the experimental data revealed a typical diffusive process following a nucleation step. The square of the front position x^2 was proportional to the time t after a short nucleation time t_0. The front mobility K could be obtained by fitting the experimental curve. Similarly, the diffusion parameters associated with the dehydrogenation process could be experimentally obtained as well.

■ MG-BASED DYNAMIC METASURFACES

Other than plasmonic color generation, in which only the amplitude of light is tailored, metasurfaces can also manipulate the phase of light at an unprecedented level. This capability has enabled a wealth of ultrathin optical devices for beam focusing and steering,[8] vortex beam generation,[68] and holography.[69]

We demonstrated a Mg-based dynamic metasurface platform that allowed independent manipulation of addressable subwavelength pixels at visible frequencies through controlled hydrogenation and dehydrogenation.[70] Such plasmonic pixels, consisting of Mg nanorods with various orientation angles, were utilized to control the light wavefronts via the Pancharatnam−Berry (PB) phase.[69] To shape arbitrary light wavefronts, eight phase levels were chosen for the metasurfaces, as shown in Figure 6A. To achieve holographic patterns with sequenced dynamics, we multiplexed the metasurface with dynamic pixels that possessed different reaction kinetics upon hydrogenation/dehydrogenation. As shown by the SEM image in Figure 6B, each unit cell

DOI: 10.1021/acs.accounts.9b00157
Acc. Chem. Res. 2019, 52, 1979−1989

contained a Mg/Pd (P_1) nanorod and a Mg/Pd/Cr (P_3) nanorod as two sets of dynamic pixels. The Cr (1 nm) capping layer could effectively decrease both the hydrogenation and dehydrogenation rates of P_3. This led to distinct time evolutions of P_1 (solid line) and P_3 (dash-dotted line) during hydrogenation and dehydrogenation (see Figure 6C). Two holographic patterns were reconstructed on the basis of P_1 and P_3 using RCP light. As shown in Figure 6D, the portrait of Marie Curie as well as the chemical symbols Po and Ra could transit among four distinct states through hydrogenation and dehydrogenation.

Taking a step further, we demonstrated dynamic Janus metasurfaces at visible frequencies.[71] Each super unit cell comprised three pixels that were categorized into two sets (see Figure 6E). In one set, a Au nanorod (P_+) and a Mg nanorod (P_-) were orthogonally arranged as counter pixels. The anomalous RCP waves reflected from P_+ and P_- achieved a π phase shift, giving rise to a reflectance minimum in the far field due to destructive interference. In the other set, there was an additional Mg nanorod (P). Before hydrogenation, the effective pixel of the super unit cell was P_e = P. After hydrogenation, Mg was transformed into MgH_2. The net function of the super unit cell was therefore only governed by P_+, i.e., $P_e = P_+$. Upon oxygen exposure, MgH_2 could be transformed back to Mg, thus restoring P_e = P. Therefore, the effective pixels on such a Janus metasurface could be reversibly regulated using H_2 and O_2, independent of the helicity of the incident light.

This scheme opened a unique pathway to endow optical metasurfaces with rich dynamic functionalities in the optical spectral region, especially for generation of metasurface holography with high security. As illustrated in Figure 6F, before hydrogenation "Y" was observed on the screen upon illumination with RCP light. After H_2 exposure, "Y" vanished, whereas "N" became visible. After O_2 exposure, "N" disappeared and "Y" reappeared. Consequently, the two holographic images containing different information could be independently reconstructed upon H_2 and O_2 exposures, respectively, while the helicity of the incident light remained unchanged.

STABILITY, REVERSIBILITY, AND DURABILITY

Mg has higher chemical reactivity than widely used plasmonic materials such as Au, Ag, and Al. Concerns about stability, reversibility, and durability as well as approaches to solve these issues are highly relevant. The corrosion kinetics of Mg under ambient conditions is mainly governed by two factors: the water content in the air and the characteristics of the Mg surface.[72] Corrosion of Mg happens rapidly in humid air. Nevertheless, it was observed that Mg films and particles are very stable when exposed to dry air because of the formation of very thin MgO passivation shells. In humid environments, MgO may absorb moisture to form $Mg(OH)_2$, which no longer serves as a protection layer for Mg. This hydration process of MgO is strongly influenced by the crystallographic orientation and the presence of defects on the oxide surface. Kooi et al. demonstrated that crystallized Mg nanoparticles exhibited a dense and crystalline MgO shell (~3 nm), preventing further oxidation under ambient conditions at room temperature for 1 month.[34] In contrast, poorly crystallized Mg with a low-density surface possessed a porous and amorphous MgO shell, which could hydride easily to form a porous $Mg(OH)_2$ layer. Therefore, improving the crystallinity of Mg during fabrication and operating Mg-based nanodevices in dry environments are critical actions to consider. To operate Mg-based nanodevices in humid air, a thin poly(tetrafluoroethylene) layer can be deposited on the Mg surface to isolate water but still allow for hydrogen diffusion.[73] In addition, for all of the aforementioned Mg-based nanodevices, the utilization of Pd and Ti capping layers was proved to be very effective for Mg protection, showing good device performance in terms of reversibility and durability.

CONCLUSION AND OUTLOOK

Mg for dynamic nanoplasmonics is a viable route to the realization of plasmonic nanodevices with novel functionalities, given its design flexibility and large modulation of the optical responses. There are remaining issues that need to be addressed for the construction of high-performance dynamic systems for real-world applications.

First, optical approaches such as s-SNOM provide physical understanding of the in situ hydrogenation and dehydrogenation processes with resolution of several tens of nanometers. Deeper insights into such processes on the atomic level can be achieved using environmental transmission electron microscopy (TEM).[74,75] For instance, Mg nanoparticles of different sizes, shapes, geometries, etc. can be fabricated by advanced EBL on an ultrathin TEM grid. Tomography and diffraction patterns of the particles before and after hydrogenation can be obtained and carefully examined. In addition, in situ electron energy loss spectropy of the Mg nanoparticles can be carried out during hydrogenation/dehydrogenation. Such characterizations will enable visualization of the phase-transition dynamics of the Mg nanoparticles in a controlled gaseous environment and allow for understanding of the fundamental atomic mechanisms of gas−solid reactions on the atomic level. In turn, the knowledge gained about the time-resolved dynamic and kinetic mechanisms on the atomic level will provide insightful blueprints for the design of Mg-based dynamic nanodevices with high performance. Second, to further improve the reversibility and durability, alloying Mg with other metals, including nickel, yttrium, vanadium, iron, etc., should be attempted.[26] Kalisvaart et al. showed that Mg films alloyed with Al, Fe, and Ti could enhance reaction kinetics and no degradation in performance was observed after 100 absorption/desorption cycles.[76] Baldi et al.[46] and Slaman et al.[45] demonstrated that Pd-capped Mg−Ti alloy films showed faster kinetics with good reversibility over 150 cycles. Remarkably, Tajima et al. reported optical switching of Mg_4Ni films over 4000 cycles.[47] Therefore, research efforts on patterning Mg alloy particles for dynamic optical nanodevices will be very rewarding to improve the device reversibility and switching rates. Third, to enhance switching rates, other hydrogenation/dehydrogenation means can be considered. Den Broeder et al. demonstrated electromigration of hydrogen in yttrium films, in which the diffusing species in the insulating yttrium trihydride was the H^- anion.[77] This concept can be applied to Mg-based systems as well, so that the hydrogenation/dehydrogenation processes in Mg can be conveniently controlled by external electric fields at high speeds. This will also eventually solve the portability issue of the gas-phase reactions.[47]

To date, Mg-based dynamic nanodevices have been utilized for applications in plasmonic chirality switching, dynamic color displays, and metasurface elements. This exploits only a glimpse of opportunities that Mg can offer. There are many

DOI: 10.1021/acs.accounts.9b00157
Acc. Chem. Res. 2019, 52, 1979−1989

interesting topics that deserve research endeavors. For instance, the out-of-plane expansion of Mg nanoparticles is as large as 30%.[38,51] This provides a unique model system to realize plasmonic devices with nanoscale mechanical responses. Also, Mg can be utilized in studies of switchable nonlinear effects, offering a tailored platform to examine the intriguing enhancement and symmetry questions in nonlinear plasmonics. Furthermore, Mg can be applied for plasmonic sensing, which is not limited only to detection of hydrogen. Rather, it can be extended to offer general dynamic platforms for tunable surface-enhanced Raman scattering, fluorescence, infrared absorption, and others. We believe that the unsolved challenges and new scientific inquires will stimulate exciting and continuous studies of Mg-based dynamic nanoplasmonics and their related applications.

AUTHOR INFORMATION

Corresponding Author

*E-mail: na.liu@kip.uni-heidelberg.de.

ORCID

Xiaoyang Duan: 0000-0002-8720-3788
Na Liu: 0000-0001-5831-3382

Author Contributions

The manuscript was written by both authors. Both authors approved the final version of the manuscript.

Notes

The authors declare no competing financial interest.

Biographies

Xiaoyang Duan is a Ph.D. candidate in Prof. Liu's group at the University of Heidelberg and the Max Planck Institute for Intelligent Systems in Germany.

Na Liu is a Professor at the Kirchhoff Institute for Physics at the University of Heidelberg in Germany.

ACKNOWLEDGMENTS

We acknowledge support from the European Research Council (ERC Dynamic Nano grant).

REFERENCES

(1) Barnes, W. L.; Dereux, A.; Ebbesen, T. W. Surface Plasmon Subwavelength Optics. *Nature* **2003**, *424*, 824−830.
(2) Schuller, J. A.; Barnard, E. S.; Cai, W.; Jun, Y. C.; White, J. S.; Brongersma, M. L. Plasmonics for Extreme Light Concentration and Manipulation. *Nat. Mater.* **2010**, *9*, 193−204.
(3) Halas, N. J.; Lal, S.; Chang, W.-S.; Link, S.; Nordlander, P. Plasmons in Strongly Coupled Metallic Nanostructures. *Chem. Rev.* **2011**, *111*, 3913−3961.
(4) Tokel, O.; Inci, F.; Demirci, U. Advances in Plasmonic Technologies for Point of Care Applications. *Chem. Rev.* **2014**, *114*, 5728−5752.
(5) Curto, A. G.; Volpe, G.; Taminiau, T. H.; Kreuzer, M. P.; Quidant, R.; van Hulst, N. F. Unidirectional Emission of a Quantum Dot Coupled to a Nanoantenna. *Science* **2010**, *329*, 930−933.
(6) Liu, N.; Liedl, T. DNA-Assembled Advanced Plasmonic Architectures. *Chem. Rev.* **2018**, *118*, 3032−3053.
(7) Kristensen, A.; Yang, J. K. W.; Bozhevolnyi, S. I.; Link, S.; Nordlander, P.; Halas, N. J.; Mortensen, N. A. Plasmonic Colour Generation. *Nat. Rev. Mater.* **2016**, *2*, 16088.
(8) Ding, F.; Pors, A.; Bozhevolnyi, S. I. Gradient Metasurfaces: A Review of Fundamentals and Applications. *Rep. Prog. Phys.* **2018**, *81*, 026401.
(9) Lal, S.; Link, S.; Halas, N. J. Nano-Optics from Sensing to Waveguiding. *Nat. Photonics* **2007**, *1*, 641−648.
(10) Krasavin, A. V.; Zheludev, N. I. Active Plasmonics: Controlling Signals in Au/Ga Waveguide Using Nanoscale Structural Transformations. *Appl. Phys. Lett.* **2004**, *84*, 1416−1418.
(11) Jiang, N.; Zhuo, X.; Wang, J. Active Plasmonics: Principles, Structures, and Applications. *Chem. Rev.* **2018**, *118*, 3054−3099.
(12) Nemati, A.; Wang, Q.; Hong, M.; Teng, J. Tunable and Reconfigurable Metasurfaces and Metadevices. *Opto-Electron. Adv.* **2018**, *1*, 180009.
(13) Kuzyk, A.; Jungmann, R.; Acuna, G. P.; Liu, N. DNA Origami Route for Nanophotonics. *ACS Photonics* **2018**, *5*, 1151−1163.
(14) Zhou, C.; Duan, X.; Liu, N. DNA-Nanotechnology-Enabled Chiral Plasmonics: From Static to Dynamic. *Acc. Chem. Res.* **2017**, *50*, 2906−2914.
(15) Urban, M. J.; Shen, C.; Kong, X.-T.; Zhu, C.; Govorov, A. O.; Wang, Q.; Hentschel, M.; Liu, N. Chiral Plasmonic Nanostructures Enabled by Bottom-Up Approaches. *Annu. Rev. Phys. Chem.* **2019**, *70*, 275−299.
(16) Wang, L.; Li, Q. Photochromism into Nanosystems: Towards Lighting up the Future Nanoworld. *Chem. Soc. Rev.* **2018**, *47*, 1044−1097.
(17) Fofang, N. T.; Grady, N. K.; Fan, Z.; Govorov, A. O.; Halas, N. J. Plexciton Dynamics: Exciton-Plasmon Coupling in a J-Aggregate-Au Nanoshell Complex Provides a Mechanism for Nonlinearity. *Nano Lett.* **2011**, *11*, 1556−1560.
(18) Gao, Y.; Huang, C.; Hao, C.; Sun, S.; Zhang, L.; Zhang, C.; Duan, Z.; Wang, K.; Jin, Z.; Zhang, N.; Kildishev, A. V.; Qiu, C.-W.; Song, Q.; Xiao, S. Lead Halide Perovskite Nanostructures for Dynamic Color Display. *ACS Nano* **2018**, *12*, 8847−8854.
(19) Liu, M.; Hwang, H. Y.; Tao, H.; Strikwerda, A. C.; Fan, K.; Keiser, G. R.; Sternbach, A. J.; West, K. G.; Kittiwatanakul, S.; Lu, J.; Wolf, S. A.; Omenetto, F. G.; Zhang, X.; Nelson, K. A.; Averitt, R. D. Terahertz-Field-Induced Insulator-to-Metal Transition in Vanadium Dioxide Metamaterial. *Nature* **2012**, *487*, 345−348.
(20) Yin, X.; Steinle, T.; Huang, L.; Taubner, T.; Wuttig, M.; Zentgraf, T.; Giessen, H. Beam Switching and Bifocal Zoom Lensing Using Active Plasmonic Metasurfaces. *Light: Sci. Appl.* **2017**, *6*, No. e17016.
(21) Si, G.; Zhao, Y.; Leong, E. S. P.; Liu, Y. J. Liquid-Crystal-Enabled Active Plasmonics: A Review. *Materials* **2014**, *7*, 1296−1317.
(22) Grigorenko, A. N.; Polini, M.; Novoselov, K. S. Graphene Plasmonics. *Nat. Photonics* **2012**, *6*, 749−758.
(23) Sanz, J. M.; Ortiz, D.; Alcaraz de la Osa, R.; Saiz, J. M.; González, F.; Brown, A. S.; Losurdo, M.; Everitt, H. O.; Moreno, F. UV Plasmonic Behavior of Various Metal Nanoparticles in the Near- and Far-Field Regimes: Geometry and Substrate Effects. *J. Phys. Chem. C* **2013**, *117*, 19606−19615.
(24) Blaber, M. G.; Arnold, M. D.; Ford, M. J. A Review of the Optical Properties of Alloys and Intermetallics for Plasmonics. *J. Phys.: Condens. Matter* **2010**, *22*, 143201.
(25) Palm, K. J.; Murray, J. B.; Narayan, T. C.; Munday, J. N. Dynamic Optical Properties of Metal Hydrides. *ACS Photonics* **2018**, *5*, 4677−4686.
(26) Sun, Y.; Shen, C.; Lai, Q.; Liu, W.; Wang, D.-W.; Aguey-Zinsou, K.-F. Tailoring Magnesium Based Materials for Hydrogen Storage through Synthesis: Current State of the Art. *Energy Storage Mater.* **2018**, *10*, 168−198.
(27) Maier, S. A. *Plasmonics: Fundamentals and Applications*; Springer: New York, 2007.
(28) Palik, E. D. *Handbook of Optical Constants of Solids*; Academic Press: New York, 1998.
(29) Krozer, A.; Kasemo, B. Hydrogen Uptake by Pd-Coated Mg: Absorption-Decomposition Isotherms and Uptake Kinetics. *J. Less-Common Met.* **1990**, *160*, 323−342.
(30) Noritake, T.; Towata, S.; Aoki, M.; Seno, Y.; Hirose, Y.; Nishibori, E.; Takata, M.; Sakata, M. Charge Density Measurement in MgH_2 by Synchrotron X-Ray Diffraction. *J. Alloys Compd.* **2003**, *356*−*357*, 84−86.

DOI: 10.1021/acs.accounts.9b00157
Acc. Chem. Res. 2019, 52, 1979−1989

(31) Huot, J.; Ravnsbæk, D. B.; Zhang, J.; Cuevas, F.; Latroche, M.; Jensen, T. R. Mechanochemical Synthesis of Hydrogen Storage Materials. *Prog. Mater. Sci.* **2013**, *58*, 30−75.

(32) Zhu, C.; Sakaguchi, N.; Hosokai, S.; Watanabe, S.; Akiyama, T. *In Situ* Transmission Electron Microscopy Observation of the Decomposition of MgH_2 Nanofiber. *Int. J. Hydrogen Energy* **2011**, *36*, 3600−3605.

(33) Kelekar, R.; Giffard, H.; Kelly, S. T.; Clemens, B. M. Formation and Dissociation of MgH_2 in Epitaxial Mg Thin Films. *J. Appl. Phys.* **2007**, *101*, 114311.

(34) Kooi, B. J.; Palasantzas, G.; De Hosson, J. T. M. Gas-Phase Synthesis of Magnesium Nanoparticles: A High-Resolution Transmission Electron Microscopy Study. *Appl. Phys. Lett.* **2006**, *89*, 161914.

(35) Appusamy, K.; Blair, S.; Nahata, A.; Guruswamy, S. Low-Loss Magnesium Films for Plasmonics. *Mater. Sci. Eng., B* **2014**, *181*, 77−85.

(36) Ares, J. R.; Leardini, F.; Díaz-Chao, P.; Ferrer, I. J.; Fernández, J. F.; Sánchez, C. Non-Isothermal Desorption Process of Hydrogenated Nanocrystalline Pd-Capped Mg Films Investigated by Ion Beam Techniques. *Int. J. Hydrogen Energy* **2014**, *39*, 2587−2596.

(37) Uchida, H. T.; Wagner, S.; Hamm, M.; Kürschner, J.; Kirchheim, R.; Hjörvarsson, B.; Pundt, A. Absorption Kinetics and Hydride Formation in Magnesium Films: Effect of Driving Force Revisited. *Acta Mater.* **2015**, *85*, 279−289.

(38) Mooij, L.; Dam, B. Hysteresis and the Role of Nucleation and Growth in the Hydrogenation of Mg Nanolayers. *Phys. Chem. Chem. Phys.* **2013**, *15*, 2782−2792.

(39) Baldi, A.; Gonzalez-Silveira, M.; Palmisano, V.; Dam, B.; Griessen, R. Destabilization of the Mg-H System through Elastic Constraints. *Phys. Rev. Lett.* **2009**, *102*, 226102.

(40) Ostenfeld, C. W.; Johansson, M.; Chorkendorff, I. Hydrogenation Properties of Catalyzed and Non-Catalyzed Magnesium Films. *Surf. Sci.* **2007**, *601*, 1862−1869.

(41) Uchida, H. T.; Kirchheim, R.; Pundt, A. Influence of Hydrogen Loading Conditions on the Blocking Effect of Nanocrystalline Mg Films. *Scr. Mater.* **2011**, *64*, 935−937.

(42) Isidorsson, J.; Giebels, I. A. M. E.; Arwin, H.; Griessen, R. Optical Properties of MgH_2 Measured *in situ* by Ellipsometry and Spectrophotometry. *Phys. Rev. B: Condens. Matter Mater. Phys.* **2003**, *68*, 115112.

(43) Gremaud, R.; Broedersz, C. P.; Borsa, D. M.; Borgschulte, A.; Mauron, P.; Schreuders, H.; Rector, J. H.; Dam, B.; Griessen, R. Hydrogenography: An Optical Combinatorial Method to Find New Light-Weight Hydrogen-Storage Materials. *Adv. Mater.* **2007**, *19*, 2813−2817.

(44) van der Sluis, P.; Ouwerkerk, M.; Duine, P. A. Optical Switches Based on Magnesium Lanthanide Alloy Hydrides. *Appl. Phys. Lett.* **1997**, *70*, 3356−3358.

(45) Slaman, M.; Dam, B.; Pasturel, M.; Borsa, D. M.; Schreuders, H.; Rector, J. H.; Griessen, R. Fiber Optic Hydrogen Detectors Containing Mg-Based Metal Hydrides. *Sens. Actuators, B* **2007**, *123*, 538−545.

(46) Baldi, A.; Borsa, D. M.; Schreuders, H.; Rector, J. H.; Atmakidis, T.; Bakker, M.; Zondag, H. A.; van Helden, W. G. J.; Dam, B.; Griessen, R. Mg-Ti-H Thin Films as Switchable Solar Absorbers. *Int. J. Hydrogen Energy* **2008**, *33*, 3188−3192.

(47) Tajima, K.; Yamada, Y.; Bao, S.; Okada, M.; Yoshimura, K. Flexible All-Solid-State Switchable Mirror on Plastic Sheet. *Appl. Phys. Lett.* **2008**, *92*, 041912.

(48) Bérubé, V.; Radtke, G.; Dresselhaus, M.; Chen, G. Size Effects on the Hydrogen Storage Properties of Nanostructured Metal Hydrides: A Review. *Int. J. Energy Res.* **2007**, *31*, 637−663.

(49) Wagemans, R. W. P.; van Lenthe, J. H.; de Jongh, P. E.; van Dillen, A. J.; de Jong, K. P. Hydrogen Storage in Magnesium Clusters: Quantum Chemical Study. *J. Am. Chem. Soc.* **2005**, *127*, 16675−16680.

(50) Sterl, F.; Strohfeldt, N.; Walter, R.; Griessen, R.; Tittl, A.; Giessen, H. Magnesium as Novel Material for Active Plasmonics in the Visible Wavelength Range. *Nano Lett.* **2015**, *15*, 7949−7955.

(51) Sterl, F.; Linnenbank, H.; Steinle, T.; Morz, F.; Strohfeldt, N.; Giessen, H. Nanoscale Hydrogenography on Single Magnesium Nanoparticles. *Nano Lett.* **2018**, *18*, 4293−4302.

(52) Chung, C.-J.; Nivargi, C.; Clemens, B. Nanometer-Scale Hydrogen 'Portals' for the Control of Magnesium Hydride Formation. *Phys. Chem. Chem. Phys.* **2015**, *17*, 28977−28984.

(53) Fasman, G. D. *Circular Dichroism and the Conformational Analysis of Biomolecules*; Springer: Boston, 1996.

(54) Hentschel, M.; Schäferling, M.; Duan, X.; Giessen, H.; Liu, N. Chiral Plasmonics. *Sci. Adv.* **2017**, *3*, No. e1602735.

(55) Matuschek, M.; Singh, D. P.; Jeong, H.-H.; Nesterov, M.; Weiss, T.; Fischer, P.; Neubrech, F.; Liu, N. Chiral Plasmonic Hydrogen Sensors. *Small* **2018**, *14*, 1702990.

(56) Zhou, C.; Xin, L.; Duan, X.; Urban, M. J.; Liu, N. Dynamic Plasmonic System That Responds to Thermal and Aptamer-Target Regulations. *Nano Lett.* **2018**, *18*, 7395−7399.

(57) Urban, M. J.; Zhou, C.; Duan, X.; Liu, N. Optically Resolving the Dynamic Walking of a Plasmonic Walker Couple. *Nano Lett.* **2015**, *15*, 8392−8396.

(58) Jeong, H.-H.; Mark, A. G.; Fischer, P. Magnesium Plasmonics for UV Applications and Chiral Sensing. *Chem. Commun.* **2016**, *52*, 12179−12182.

(59) Guerrero-Martínez, A.; Auguié, B.; Alonso-Gómez, J. L.; Džolić, Z.; Gómez-Graña, S.; Žinić, M.; Cid, M. M.; Liz-Marzán, L. M. Intense Optical Activity from Three-Dimensional Chiral Ordering of Plasmonic Nanoantennas. *Angew. Chem., Int. Ed.* **2011**, *50*, 5499−5503.

(60) Kuzyk, A.; Schreiber, R.; Fan, Z.; Pardatscher, G.; Roller, E.-M.; Högele, A.; Simmel, F. C.; Govorov, A. O.; Liedl, T. DNA-Based Self-Assembly of Chiral Plasmonic Nanostructures with Tailored Optical Response. *Nature* **2012**, *483*, 311−314.

(61) Duan, X.; Kamin, S.; Sterl, F.; Giessen, H.; Liu, N. Hydrogen-Regulated Chiral Nanoplasmonics. *Nano Lett.* **2016**, *16*, 1462−1466.

(62) Duan, X.; Yue, S.; Liu, N. Understanding Complex Chiral Plasmonics. *Nanoscale* **2015**, *7*, 17237−17243.

(63) Kumar, K.; Duan, H.; Hegde, R. S.; Koh, S. C. W.; Wei, J. N.; Yang, J. K. W. Printing Colour at the Optical Diffraction Limit. *Nat. Nanotechnol.* **2012**, *7*, 557−561.

(64) Duan, X.; Kamin, S.; Liu, N. Dynamic Plasmonic Colour Display. *Nat. Commun.* **2017**, *8*, 14606.

(65) Chen, Y.; Duan, X.; Matuschek, M.; Zhou, Y.; Neubrech, F.; Duan, H.; Liu, N. Dynamic Color Displays Using Stepwise Cavity Resonators. *Nano Lett.* **2017**, *17*, 5555−5560.

(66) Duan, X.; Liu, N. Scanning Plasmonic Color Display. *ACS Nano* **2018**, *12*, 8817−8823.

(67) Duan, X.; Griessen, R.; Wijngaarden, R. J.; Kamin, S.; Liu, N. Self-Recording and Manipulation of Fast Long-Range Hydrogen Diffusion in Quasifree Magnesium. *Phys. Rev. Mater.* **2018**, *2*, 085802.

(68) Yu, N.; Genevet, P.; Kats, M. A.; Aieta, F.; Tetienne, J.-P.; Capasso, F.; Gaburro, Z. Light Propagation with Phase Discontinuities: Generalized Laws of Reflection and Refraction. *Science* **2011**, *334*, 333−337.

(69) Zheng, G.; Muhlenbernd, H.; Kenney, M.; Li, G.; Zentgraf, T.; Zhang, S. Metasurface Holograms Reaching 80% Efficiency. *Nat. Nanotechnol.* **2015**, *10*, 308−312.

(70) Li, J.; Kamin, S.; Zheng, G.; Neubrech, F.; Zhang, S.; Liu, N. Addressable Metasurfaces for Dynamic Holography and Optical Information Encryption. *Sci. Adv.* **2018**, *4*, No. eaar6768.

(71) Yu, P.; Li, J.; Zhang, S.; Jin, Z.; Schutz, G.; Qiu, C.-W.; Hirscher, M.; Liu, N. Dynamic Janus Metasurfaces in the Visible Spectral Region. *Nano Lett.* **2018**, *18*, 4584−4589.

(72) Nordlien, J. H.; Ono, S.; Masuko, N.; NişancioǦlu, K. Morphology and Structure of Oxide Films Formed on Magnesium by Exposure to Air and Water. *J. Electrochem. Soc.* **1995**, *142*, 3320−3322.

DOI: 10.1021/acs.accounts.9b00157
Acc. Chem. Res. 2019, 52, 1979−1989

(73) Ngene, P.; Westerwaal, R. J.; Sachdeva, S.; Haije, W.; de Smet, L. C. P. M.; Dam, B. Polymer-Induced Surface Modifications of Pd-Based Thin Films Leading to Improved Kinetics in Hydrogen Sensing and Energy Storage Applications. *Angew. Chem., Int. Ed.* **2014**, *53*, 12081−12085.
(74) Narayan, T. C.; Baldi, A.; Koh, A. L.; Sinclair, R.; Dionne, J. A. Reconstructing Solute-Induced Phase Transformations within Individual Nanocrystals. *Nat. Mater.* **2016**, *15*, 768−774.
(75) Biggins, J. S.; Yazdi, S.; Ringe, E. Magnesium Nanoparticle Plasmonics. *Nano Lett.* **2018**, *18*, 3752−3758.
(76) Kalisvaart, W. P.; Harrower, C. T.; Haagsma, J.; Zahiri, B.; Luber, E. J.; Ophus, C.; Poirier, E.; Fritzsche, H.; Mitlin, D. Hydrogen Storage in Binary and Ternary Mg-Based Alloys: A Comprehensive Experimental Study. *Int. J. Hydrogen Energy* **2010**, *35*, 2091−2103.
(77) den Broeder, F. J. A.; van der Molen, S. J.; Kremers, M.; Huiberts, J. N.; Nagengast, D. G.; van Gogh, A. T. M.; Huisman, W. H.; Koeman, N. J.; Dam, B.; Rector, J. H.; Plota, S.; Haaksma, M.; Hanzen, R. M. N.; Jungblut, R. M.; Duine, P. A.; Griessen, R. Visualization of Hydrogen Migration in Solids Using Switchable Mirrors. *Nature* **1998**, *394*, 656−658.

DOI: 10.1021/acs.accounts.9b00157
Acc. Chem. Res. 2019, 52, 1979−1989